

# Journal of Materials Chemistry A

Accepted Manuscript



This is an *Accepted Manuscript*, which has been through the Royal Society of Chemistry peer review process and has been accepted for publication.

*Accepted Manuscripts* are published online shortly after acceptance, before technical editing, formatting and proof reading. Using this free service, authors can make their results available to the community, in citable form, before we publish the edited article. We will replace this *Accepted Manuscript* with the edited and formatted *Advance Article* as soon as it is available.

You can find more information about *Accepted Manuscripts* in the [Information for Authors](#).

Please note that technical editing may introduce minor changes to the text and/or graphics, which may alter content. The journal's standard [Terms & Conditions](#) and the [Ethical guidelines](#) still apply. In no event shall the Royal Society of Chemistry be held responsible for any errors or omissions in this *Accepted Manuscript* or any consequences arising from the use of any information it contains.

## COMMUNICATION

Assessment of polyanion ( $\text{BF}_4^-$  and  $\text{PF}_6^-$ ) substitutions in hybrid halide perovskites

Cite this: DOI: 10.1039/x0xx00000x

Christopher H. Hendon, Ruo Xi Yang, Lee A. Burton, and Aron Walsh\*

Received 00th January 2012,  
Accepted 00th January 2012

DOI: 10.1039/x0xx00000x

www.rsc.org/

Halide perovskites have attracted attention for light-to-electricity conversion in solar cells due to their favorable optoelectronic properties. In particular, the replacement of the *A* cation by an isovalent molecule has proven highly successful. We explore the substitution of the *X* anion, producing polyanion perovskites based on hexafluorophosphate and tetrafluoroborate. Starting from  $\text{CsPbI}_3$ , the effect of partial and complete substitution is investigated using relativistic electronic structure calculations.  $\text{BF}_4^-$  results in a larger perturbation to the electronic structure than  $\text{PF}_6^-$ ; however, both localise the band edge states, and the end member compounds are predicted to be wide band gap dielectrics.

The characteristic structural motif of the perovskite ( $\text{ABX}_3$ ) crystal structure is a corner-sharing array of  $\text{BX}_6$  octahedra. The three-dimensional arrangement of these octahedra gives rise to a range of polymorphs (i.e. the four tilt systems dictated by Glazer<sup>1</sup>). The 12-coordinate hole formed at the centre of each octahedral cage is occupied by a cation at the *A* site (see Figure 1).

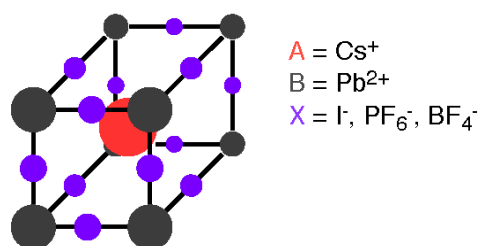


**Fig. 1.** Schematic of the perovskite crystal structure composed of two cations (*A* and *B*) and an anion (*X*). Here we consider both elemental and molecular anions.

For charge neutrality of the material, the simple rule is that the formal oxidation states of the cations (*A*+*B*) balance those of

the anions (*3X*). While oxide perovskites are the most widely studied (i.e.  $A+B=VI$ ), there are many examples of halide perovskites (i.e.  $A+B=III$ ). There are fewer allowed metal combinations for the halides, with the typical case being  $A=I$  and  $B=II$ , e.g.  $\text{NaFeF}_3$ . In addition to charge, geometric constraints restrict the range of possible compositions. These are summarised by the radius ratio rules as defined by the Goldschmidt tolerance factor<sup>2</sup>:

$$\alpha = \frac{r_A + r_X}{\sqrt{2}(r_B + r_X)}$$

which depends on the ionic radius of each component of the perovskite. Stable perovskite materials are usually found in the range  $0.7 < \alpha < 1$ . For example, for  $\text{CsPbI}_3$  the value is 0.85 based on the effective ionic radii proposed by Shannon<sup>3</sup>.

In addition to inorganic perovskite solid-solutions and ordered-defect structures, a diverse family of hybrid perovskites are also known to exist<sup>4</sup>. In the simplest case, the *A* metal is replaced by an isovalent molecule and the  $\text{BX}_3$  connectivity is maintained. A popular example is  $\text{CH}_3\text{NH}_3\text{PbI}_3$ , where  $\alpha = 0.91$ .<sup>5</sup> There are many examples of where 2D and 1D networks are formed due to steric factors<sup>6</sup>. More exotic 'perovskite like' metal-organic frameworks also exist, e.g. the bimetallic azido systems (e.g.  $\text{N}(\text{CH}_3)_4)_2[\text{Cr}, \text{Na}(\text{N}_3)_6]$ <sup>7</sup>.

One recent driving force for the study of halide perovskites has been in photovoltaics, where both inorganic (e.g.  $\text{CsSnI}_3$ ) and hybrid (e.g.  $\text{CH}_3\text{NH}_3\text{PbI}_3$ ) perovskites have demonstrated high power conversion efficiencies for low-temperature solution-processed materials<sup>8–10</sup>. The remarkable performance can be attributed to the combination of strong optical absorption, light carrier effective masses, large dielectric constants and, currently less well understood, ferroelectricity.<sup>11,12</sup>

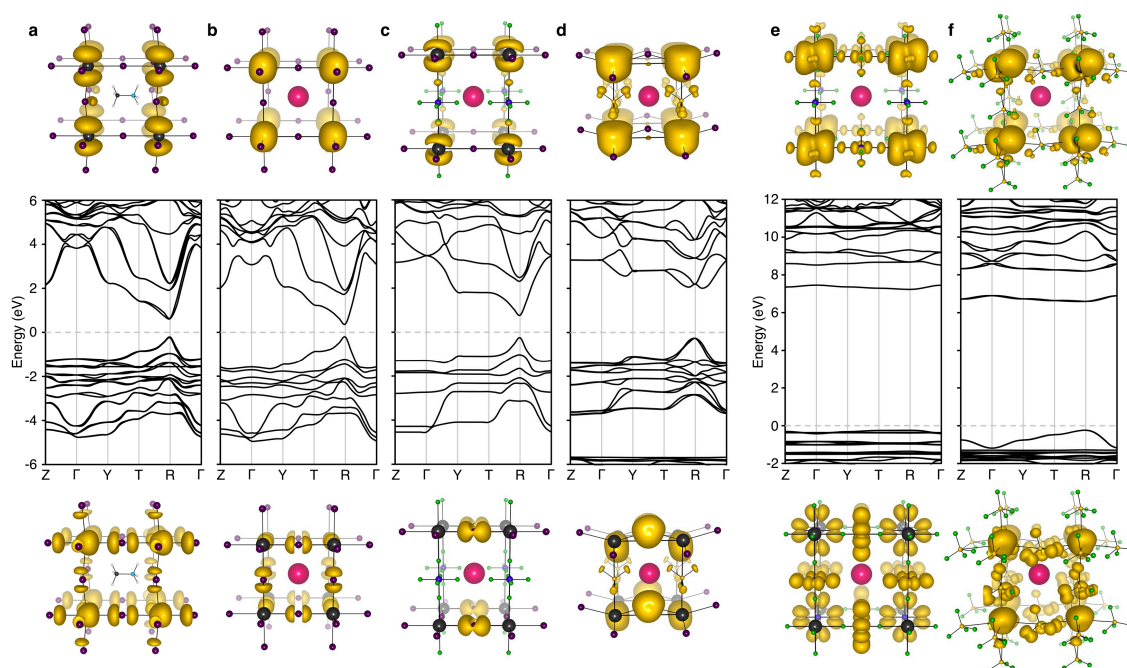


**Fig. 2.** Electronic band structure (DFT/HSE06 including spin-orbit coupling) of (a)  $\text{CH}_3\text{NH}_3\text{PbI}_3$  (b)  $\text{CsPbI}_3$ , (c)  $\text{CsPb}[\text{I}_2][\text{PF}_6]$ , (d)  $\text{CsPb}[\text{I}_2][\text{BF}_4]$ , (e)  $\text{CsPb}[\text{PF}_6]_3$  and (f)  $\text{CsPb}[\text{BF}_4]_3$ . The structure for (a) is taken from Ref. <sup>28</sup> and corresponds to the  $\langle 100 \rangle$  pseudo-cubic orientation of methylammonium. Shown below and above the bandstructures are the charge density isosurfaces of the valence band maximum and conduction band minimum, respectively. Visualization is performed in the code *VESTA*.<sup>29</sup> Note that for the partial polyanion substitutions (c – d), the band gap remains at the  $R$  point ( $\frac{1}{2}, \frac{1}{2}, \frac{1}{2}$ ) of the Brillouin zone. Strong relativistic Dresselhaus splitting is predicted for the lower conduction band of (d) due to the breaking of inversion symmetry associated with the  $\text{BF}_4$  anion.

In this Communication, we consider hybrid halide perovskites from a different perspective: the hybrid solid formed by substituting the *anion*, rather than the *cation*. Specifically, we investigate  $\text{CsPbX}_3$  ( $X = \text{I}, \text{PF}_6$  and  $\text{BF}_4$ ) including partial and complete substitutions. The crystal structures and electronic properties are predicted by a first-principles method. The successful synthesis of  $\text{BF}_4$  incorporated  $\text{CH}_3\text{NH}_3\text{PbI}_3$  was recently reported<sup>13</sup>, which highlights that even more complex “double hybrid” compounds are possible to synthesise.

Calculations were performed using density functional theory in the code *VASP*<sup>14,15</sup>. A two-step procedure was adopted, with structure optimisation at the level of *PBEsol*<sup>16</sup> and electronic structure analysis with the non-local HSE06 exchange-correlation functional including 25% screened Hartree-Fock exchange<sup>17,18</sup>. The basis set (500 eV cutoff), k-points ( $6 \times 6 \times 6$ ) and internal forces ( $1 \text{ meV}/\text{\AA}^3$ ) were converged for the properties of interest. Particular care was given to relativistic effects, which are known to be large for Pb-containing compounds: scalar relativistic corrections were included in the projector-augmented wave core potentials and spin-orbit interactions were treated for the valence electrons. The optimised crystal structures are available in an on-line repository<sup>19</sup>. The effective masses were determined using the package Boltztrap<sup>20</sup> via Pymatgen<sup>21</sup>.

It should be noted that the computed band gap values reported here (see Table 1) are qualitative for two reasons: (i) many body effects are particularly large in these systems, which can renormalize both the band gap and band dispersion;<sup>22</sup> (ii) the cubic perovskite lattice may represent an average structure that is subject to effects from dynamic disorder (local symmetry breaking).<sup>23</sup> The general trends are expected to be reliable.

The cubic perovskite structure of  $\text{CsPbI}_3$  has octahedral symmetry (space group  $Pm-3m$ ) and the iodide sites have linear coordination with respect to Pb. The tolerance factor of 0.85 is insensitive to the polyanion substitutions considered here (Table 1). For the octahedral  $\text{PF}_6$  anion, the linear coordination is maintained through the axial termini, which maintains cubic perovskite symmetry for  $\text{CsPb}[\text{PF}_6]_3$ . For the tetrahedral  $\text{BF}_4$  anion, the linear coordination is symmetric through two edges of the tetrahedron and is thus not in line with any B-F bond ( $C_s$  symmetry, space group  $C1m1$ ).

The lattice parameter of  $\text{CsPbI}_3$  is increased by 8% and 30% for  $\text{BF}_4$  and  $\text{PF}_6$ , respectively, due to their larger effective ionic radii (see Table I). Two partially substituted structures were also considered with one (001) layer of iodine replaced by the respective polyanion. The equilibrium crystal structures exhibit a tetragonal distortion ( $a/c$ ) of 0.91 ( $\text{BF}_4$ ) and 0.74 ( $\text{PF}_6$ ). For  $\text{BF}_4$ , the Pb-I chains are also perturbed, with the bond angle decreasing from 180 to 149°.

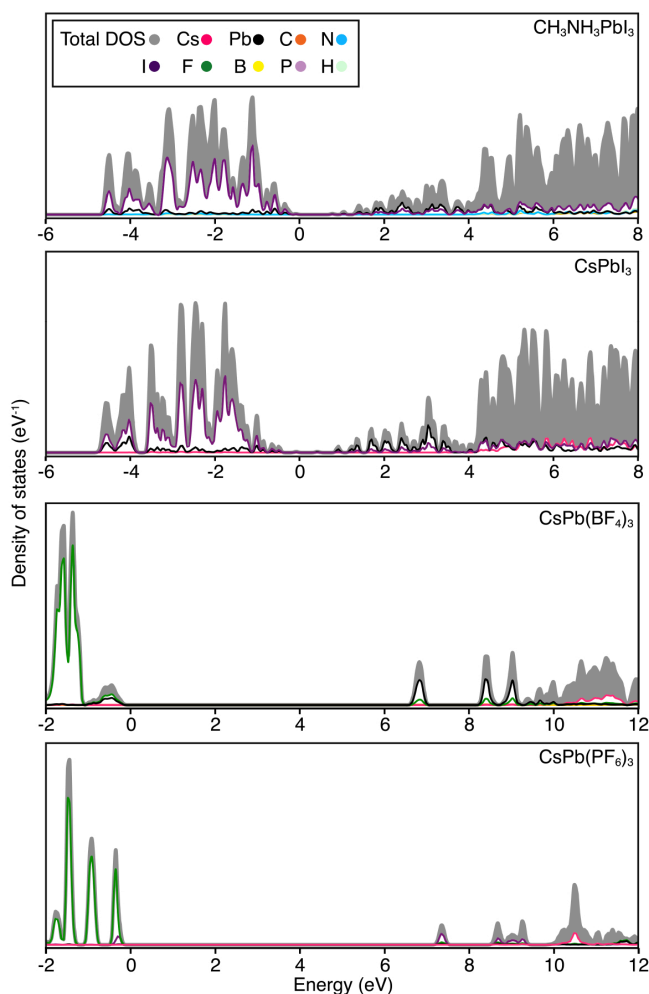


**Fig. 3.** Electronic density of states are shown for  $\text{CH}_3\text{NH}_3\text{PbI}_3$ ,  $\text{CsPbI}_3$ ,  $\text{CsPb}(\text{BF}_4)_3$  and  $\text{CsPb}(\text{PF}_6)_3$ . The top of the valence band is set to 0 eV in each case, and the partial ion contributions are determined from a spherical integration around each lattice site. The similarity between the electronic structure for Cs and  $\text{CH}_3\text{NH}_3$  compounds has previously been noted.<sup>30</sup> For the polyanion compounds, the band gaps are widened and the band edges become more localized, in accordance with the band structures shown in Fig. 2.

The electronic structure of  $\text{CsPbI}_3$  follows the oxidation states of the elements: Cs(I) is electronically inert; Pb(II) has a filled 6s band and an empty 6p band; iodide has a complete 5p shell. Therefore, the upper valence and lower conduction bands – key for hole and electron transport – are formed by the overlap of Pb 6s/I 5p and Pb 6p atomic orbitals, respectively. The corresponding charge density profiles are drawn in Figure 2, and the electronic density of states provided in Figure 3.

In these structures, the occupied Pb 6s electrons are stereochemically “inactive”, but the formation of a direct lone pair can occur and is associated with the ferroelectric activity of Pb(II) containing materials<sup>24</sup>.  $\text{CsPbI}_3$  exhibits significant band

dispersion in reciprocal space, corresponding to light hole effective masses ( $0.16 m_e$ ), which are comparable to the solar cell absorber  $\text{CH}_3\text{NH}_3\text{PbI}_3$  ( $0.20 m_e$ ; further decreased to  $0.12 m_e$  with many body corrections)<sup>22</sup>. A direct band gap is predicted at the boundary of the first Brillouin zone ( $R$  point) in agreement with other studies<sup>25,26</sup>.

**Table 1.** Empirical Goldschmidt tolerance factor ( $\alpha$ ) and electronic properties of the perovskites predicted from DFT/HSE06+SOC. The equilibrium pseudo-cubic cell parameter ( $a^* = \sqrt[3]{a \times b \times c}$  from DFT/PBESol), the electronic band gap ( $E_g$ ), and the average of the effective mass tensor of the valence band are each listed. See the note in text regarding the qualitative nature of the band gap values reported here.

| Material                               | $\alpha$ | $a^*$ (Å) | $E_g$ (eV) | $m_h^*$ ( $m_e$ ) |
|--|----------|-----------|------------|-------------------|
| $\text{CH}_3\text{NH}_3\text{PbI}_3$   | 0.91     | 6.29      | 0.81       | 0.20              |
| $\text{CsPbI}_3$                       | 0.85     | 6.26      | 0.51       | 0.16              |
| $\text{CsPb}[\text{I}_2][\text{PF}_6]$ | 0.85     | 6.83      | 1.07       | 0.41              |
| $\text{CsPb}[\text{I}_2][\text{BF}_4]$ | 0.85     | 6.22      | 2.37       | 8.67              |
| $\text{CsPb}[\text{PF}_6]_3$           | 0.84     | 8.11      | 7.47       | 4.62              |
| $\text{CsPb}[\text{BF}_4]_3$           | 0.85     | 6.75      | 6.83       | 4.41              |

For the layered compounds, the first notable change in electronic structure is the anisotropy in the chemical bonding. Band dispersion is significantly reduced along the stacking direction ( $\Gamma$  to  $Z$  in Figure 2). It is clear that the molecular orbitals of the polyanion groups hybridise less strongly with the atomic orbitals of Pb. The magnitudes of the band gaps are therefore increased (with decreased band widths). The upper valence band is still dominated by I 5p, but the bonding is in 2D sheets rather than a 3D network. The conduction band remains formed by Pb 6p orbitals, while again the connectivity is modified.

For the complete polyanion substitutions, the band structures show almost no dispersion in reciprocal space, and the density of states becomes more localised. Due to reduced bandwidths, the band gaps are further blue-shifted to the deep UV region ( $> 6$  eV). Here the contributions to the upper valence band are solely from the molecular orbitals of the polyanions. Correspondingly, the hole effective masses are heavier than the free electron mass. These materials will be electrically inert and insulating or poorly conducting in the polaronic “hopping” limit. The suggestion that the substitution of  $\text{I}^-$  by  $\text{BF}_4^-$  leads to hole doping is erroneous<sup>13</sup>.

Considering the limited range of possible halide perovskite materials, the use of polyanions presents a simple route to further extending their optoelectronic properties. Replacement of chemically reactive halides by more robust polyanions also provides a mechanism to enhance stability. This approach has led to great success in the development of electrodes for lithium batteries<sup>27</sup>. For the two cases studied here, band gaps are increased to shorter wavelengths. Anion engineering could be useful for spectral tuning of multi-junction absorber materials

for solar cells, in the dilute regime, or for producing selective electron or hole blocking layers. For the end member compounds, the increased transparency may be exploited as luminescent host materials, e.g. for phosphors, or as dielectric layers in electrical devices.

## Conclusions

A computational exploration, combined with the recent synthesis of BF<sub>4</sub> incorporated CH<sub>3</sub>NH<sub>3</sub>PbI<sub>3</sub>, has highlighted the chemical versatility of multi-component perovskites. These materials are most commonly solution processed at low temperatures in a kinetic regime that can allow for thermodynamically metastable structures to be synthesized. While *ab initio* screening of the global stability of a material is challenging in this case, it does vastly increase the range of potential hybrid structures. The recent application of the Goldschmidt tolerance factor to hybrid perovskites has suggested a range of plausible compositions<sup>5</sup>. Extension to polyanion systems predicts that larger organic cations such as imidazolium and dimethylammonium are optimal for maintaining a perovskite network ( $\alpha \sim 1$ ) with BF<sub>4</sub> and PF<sub>6</sub> anions. The combination of molecular cations and polyanions in a single framework opens up an array of possibilities that can be exploited for functional materials design and optimization.

The authors thank A. T. Murray for insightful remarks. We acknowledge membership of the U.K.'s HPC Materials Chemistry Consortium, which is funded by EPSRC Grant EP/F067496. Additional support has been received from EPSRC Grants EP/K016288/1 and EP/J017361/1, the Royal Society and the ERC (Grant 277757).

## Notes and references

<sup>a</sup> Centre for Sustainable Chemical Technologies and Department of Chemistry, University of Bath, Claverton Down, Bath BA2 7AY, UK

E-mail: [a.walsh@bath.ac.uk](mailto:a.walsh@bath.ac.uk)

Electronic Supplementary Information (ESI) available: Crystallographic information files for each of the equilibrium crystal structures. See DOI: 10.1039/c000000x/

1. A. M. Glazer, *Acta Crystallogr. Sect. B Struct. Crystallogr. Cryst. Chem.*, 1972, **28**, 3384–3392.
2. V. M. Goldschmidt, *Naturwissenschaften*, 1926, **14**, 477–485.
3. R. Shannon, *Acta Crystallogr. Sect. A Cryst. Physics*, 1976, **A32**, 751.
4. D. B. Mitzi, *J. Chem. Soc. Dalton Trans.*, 2001, 1–12.
5. G. Kieslich, S. Sun, and A. K. Cheetham, *Chem. Sci.*, 2014, **Advance Article**.
6. D. B. Mitzi, S. Wang, C. A. Feild, C. A. Chess, and A. M. Guloy, *Science* 1995, **267**, 1473–1476.
7. Z.-Y. Du, Y.-P. Zhao, C.-T. He, B.-Y. Wang, W. Xue, H.-L. Zhou, J. Bai, B. Huang, W.-X. Zhang, and X.-M. Chen, *Cryst. Growth Des.*, 2014, **Advance Article**.
8. M. M. Lee, J. Teuscher, T. Miyasaka, T. N. Murakami, and H. J. Snaith, *Science*, 2012, **643**.
9. J. M. Ball, M. M. Lee, A. Hey, and H. J. Snaith, *Energy Environ. Sci.*, 2013, 1739–1743.
10. G. Eperon and S. Stranks, *Energy Environ. Sci.*, 2014, **7**, 982.
11. J. M. Frost, K. T. Butler, F. Brivio, C. H. Hendon, M. van Schilfgaarde, and A. Walsh, *Nano Lett.*, 2014, **14**, 2584–2590.
12. Y. Kutes, L. Ye, Y. Zhou, S. Pang, B. D. Huey, and N. P. Padture, *J. Phys. Chem. Lett.*, 2014, **Advance Article**.
13. S. Nagane, U. Bansode, O. Game, S. Y. Chhatre, and S. Ogale, *Chem. Commun.*, 2014, **50**, 9741.
14. J. Paier, M. Marsman, K. Hummer, G. Kresse, I. C. Gerber, and J. G. Angyan, *J. Chem. Phys.*, 2006, **124**, 154709–13.
15. G. Kresse and J. Furthmüller, *Phys. Rev. B*, 1996, **54**, 11169.
16. J. P. Perdew, A. Ruzsinszky, G. I. Csonka, O. A. Vydrov, G. E. Scuseria, L. A. Constantin, X. Zhou, and K. Burke, *Phys. Rev. Lett.*, 2008, **100**, 136406–4.
17. J. Heyd, G. E. Scuseria, and M. Ernzerhof, *J. Chem. Phys.*, 2003, **118**, 8207.
18. J. Heyd, G. E. Scuseria, and M. Ernzerhof, *J. Chem. Phys.*, 2006, **124**, 219906–1.
19. <https://github.com/WMD-Bath/Hybrid-perovskites> (Accessed 1st April 2014)
20. G. Madsen and D. Singh, *Comput. Phys. Commun.*, 2006, **175**, 67–71.
21. A. Jain, S. P. Ong, G. Hautier, W. Chen, W. D. Richards, S. Dacek, S. Cholia, D. Gunter, D. Skinner, G. Ceder, and K. A. Persson, *APL Mater.*, 2013, **1**, 011002.
22. F. Brivio, K. T. Butler, A. Walsh, and M. van Schilfgaarde, *Phys. Rev. B*, 2014, **89**, 155204.
23. M. Dove, *Am. Mineral.*, 1997, **82**, 213–244.
24. A. Walsh, D. J. Payne, R. G. Egdell, and G. W. Watson, *Chem. Soc. Rev.*, 2011, **40**, 4455–4463.
25. L. Lang, J.-H. Yang, H.-R. Liu, H. J. Xiang, and X. G. Gong, *Phys. Lett. A*, 2014, **378**, 290–293.
26. Y. Chang, C. Park, and K. Matsuishi, *J. Korean Phys. Soc.*, 2004, **44**, 889–893.
27. M. S. Islam and C. A. J. Fisher, *Chem. Soc. Rev.*, 2014, **43**, 185–204.
28. F. Brivio, A. B. Walker, and A. Walsh, *APL Mater.*, 2013, **1**, 042111.
29. K. Momma and F. Izumi, *J. Appl. Crystallogr.*, 2011, **44**, 1272–1276.
30. J. Even and L. Pedesseau, *J. Phys. Chem. Lett.*, 2013, **4**, 2999.



The incorporation of tetrafluoroborate and hexafluorophosphate in halide perovskites are found to result in substantial band gap widening.  
80x39mm (300 x 300 DPI)